Applied Surface Science 316 (2014) 222–231

Contents lists available at ScienceDirect

Applied Surface Science

journal homepage: www.elsevier.com/locate/apsusc

Preparation and icephobic properties of polymethyltrifluoropropylsiloxane–polyacrylate block copolymers

Xiaohui Li [a], Yunhui Zhao [a], Hui Li [b], Xiaoyan Yuan [a,*]

[a] School of Materials Science and Engineering, and Tianjin Key Laboratory of Composite and Functional Materials, Tianjin University, Tianjin 300072, China
[b] School of Chemistry and Chemical Engineering, Shandong Key Laboratory of Fluorine Chemistry and Chemical Engineering Materials, University of Jinan, Jinan 250022, China

ARTICLE INFO

Article history:
Received 11 April 2014
Received in revised form 16 July 2014
Accepted 17 July 2014
Available online 25 July 2014

Keywords:
PMTFPS–*b*-polyacrylate
Microphase separation
Surface composition
Icephobicity
Synergistic effect of silicone and fluorine

ABSTRACT

Five polymethyltrifluoropropylsiloxane (PMTFPS)–polyacrylate block copolymers (PMTFPS–*b*-polyacrylate) were synthesized by free radical polymerization of methyl methacrylate, *n*-butyl acrylate and hydroxyethyl methacrylate using PMTFPS macroazoinitiator (PMTFPS-MAI) in range of 10–50 mass percentages. The morphology, surface chemical composition and wettability of the prepared copolymer films were investigated by transmission electron microscopy, atomic force microscopy, X-ray photoelectron spectroscopy, and water contact angle measurement. Delayed icing time and ice shear strength of the films were also detected for the icephobic purpose. The surface morphologies of the copolymers were different from those of the bulk because of the migration of the PMTFPS segments to the air interface during the film formation. Maximal delayed icing time (186 s at −15 °C) and reduction of the ice shear strength (301 ± 10 kPa) which was significantly lower than that of polyacrylates (804 ± 37 kPa) were achieved when the content of PMTFPS-MAI was 20 wt%. The icephobicity of the copolymers was attributed primarily to the enrichment of PMTFPS on the film surface and synergistic effect of both silicone and fluorine. Thus, the results show that the PMTFPS–*b*-polyacrylate copolymer can be used as icephobic coating materials potentially.

1. Introduction

Ice adhesion on exposed surfaces such as aircrafts, wind turbines, and downed power lines may cause severe accidents [1]. Icephobic coating has recently been proposed as an important and promising passive technique to reduce ice accumulation or ice adhesion on exposed surfaces. It is well known that superhydrophobic coatings with water contact angles of above 150° may effectively inhibit water accumulation on the surfaces [2–6]. However, formation of frost on superhydrophobic surfaces in highly humid atmospheres may negate the icephobic characteristics of superhydrophobic coatings [7–9]. Because of the interlocking between the ice and textured surface, the adhesion strength of ice on the superhydrophobic surface is much larger than that on the smooth surface, which limits the utility of superhydrophobic coating as icephobic materials [10,11].

Distinct icephobic performance has been demonstrated by low surface energy coatings, including silicone-based polymers and fluoropolymers [12–17]. Poly(dimethylsiloxane) (PDMS), which has a low surface energy (22.7 mJ m^{-2}) and low glass transition temperature (T_g, −123 °C), exhibits good icephobic properties [18,19]. Because of the weak interaction and dissimilar rheological–mechanical properties between the coating and the ice, the PDMS-based polymer can reduce the ice adhesion strength, which makes it a good candidate for icephobic coatings. In our previous study, it was proved that the ice adhesion strength could be decreased by the contribution of PDMS in polyacrylate–PDMS copolymers [20]. Fluoropolymers with extremely low surface energy may also be used as icephobic materials. Moreover, fluoropolymers tend to adhere preferably on the substrate and also show better mechanical properties than PDMS. Because of their low permittivity ($\varepsilon \approx 2.1$), fluoropolymers can reduce the electrostatic force between the substrate and the ice, resulting in low ice adhesion strength [21]. However, both PDMS-based polymers and fluoropolymers have drawbacks as icephobic coatings; e.g., the former shows poor mechanical properties and low oil repellency, while the latter has a high T_g value.

The interaction energy between the fluorocarbon group and water is three times larger than that of the

* Corresponding author. Tel.: +86 22 8740 1870; fax: +86 22 8740 1870.
E-mail addresses: xyuan28@yahoo.com, yuanxy@tju.edu.cn (X. Yuan).

http://dx.doi.org/10.1016/j.apsusc.2014.07.097
0169-4332/

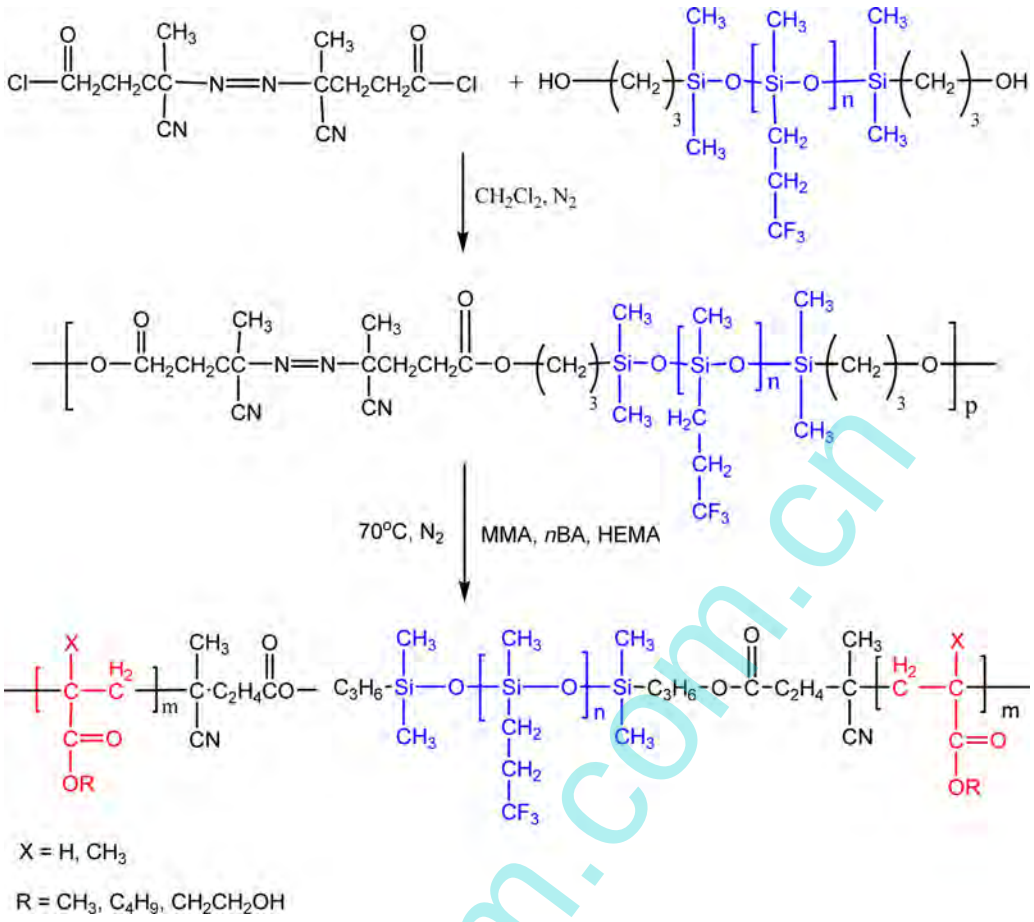

Fig. 1. Synthesis of the PMTFPS–*b*-polyacrylate copolymers.

siloxane group and water [22]. For heterogeneous polymer surfaces containing siloxane groups and flurorcarbon, the interaction energies between the polymer surface and water would decrease when both the siloxane groups and fluorocarbon are close to a water molecule. Thus, the synergistic effect of silicone and fluorine would lead to low ice adhesion strength.

Fortunately, fluorosilicones combining the advantages of fluoropolymer and silicone, could possibly surmount their individual weakness [23]. Fluorosilicone-based copolymers have the distinguishing features of chemical inertness, thermal stability and low temperature flexibility, and thus they may be used as ice or snow repellent coatings [24]. In contrast, although acrylate polymers exhibit good mechanical properties and adhesive performance, their applications are limited by poor water/oil resistance and thermal stability. Introduction of fluorosilicone into acrylate polymers may lead to the improved surface properties. So far, a well-known fluorosilicone, polymethyltrifluoropropylsiloxane (PMTFPS) which incorporates fluorinated alkyl group into the polysiloxane chain, has not been systematically studied as icephobic materials.

In this study, five PMTFPS-polyacrylate copolymers (PMTFPS–*b*-polyacrylate) were synthesized by free radical polymerization of methyl methacrylate (MMA), *n*-butyl acrylate (*n*BA) and hydroxyethyl methacrylate (HEMA) using PMTFPS macroazoinitiator (PMTFPS-MAI) in 10–50 of mass percentage. The morphologies and surface chemical compositions of the copolymer films, as well as the effect of the PMTFPS block on the water freezing process and ice adhesion, were investigated.

2. Experimental methods

2.1. Materials

α,ω-Dihydrogen-terminated polymethyltrifluoropropylsiloxane (H-PMTFPS-H) with relative molar mass of about 2000 was supplied by Shanghai Silicon Mountain Macromolecular Materials Co., Ltd., China. 4,4′-Azobis(4-cyanovaleric acid) (ACVAc) and platinum divinyltetramethyldisiloxane complex in xylene were purchased from Sigma–Aldrich. *n*BA, MMA, HEMA, oxalyl chloride, allyl alcohol and solvents including methyl isobutyl ketone (MIBK), butyl acetate (BEA), ethyl acetate (EA), dichloromethane (DCM) were purchased from Kemiou Chemical Co., Tianjin, China. MMA, BA and HEMA were purified by passing over a column of alumina to remove inhibitor. DCM and EA were dried with 3-A molecular sieves. Other chemicals were used as received without further purification.

2.2. Synthesis

Five PMTFPS–*b*-polyacrylate block copolymers were synthesized by free radical polymerization of MMA, *n*BA and HEMA with PMTFPS-MAI in 10–50 wt% (Fig. 1). PMTFPS-MAI was prepared from hydroxyl-terminated PMTFPS (HO-PMTFPS-OH) and 4,4′-azobis(cyanovalerianic acid chloride) by condensation reaction, whereas HO-PMTFPS-OH and 4,4′-azobis(cyanovalerianic acid chloride) were synthesized according to the references [25–27]. Briefly, HO-PMTFPS-OH was reacted with equimolar 4,4′-azobis(cyanovalerianic acid chloride) under N_2 protection in DCM

Table 1
Compositions, relative molar mass and yield of the PMTFPS–*b*-polyacrylate copolymers.

Sample[a]	PMTFPS-MAI	AIBN	Monomer (g)			$\bar{M}_n$	$\bar{M}_w$	$\bar{M}_w/\bar{M}_n$	Yield
	(g)	(g)	MMA	BA	HEMA	($\times 10^4$)	($\times 10^4$)		(%)
P1	0.30	–	1.5	1.0	0.2	3.23	5.84	1.81	60.0
P2	0.68	–	1.5	1.0	0.2	2.32	4.03	1.73	75.7
P3	1.16	–	1.5	1.0	0.2	2.20	3.81	1.72	80.1
P4	1.80	–	1.5	1.0	0.2	1.92	3.08	1.60	85.2
P5	2.70	–	1.5	1.0	0.2	1.52	2.43	1.59	87.2
PMTFPS	–	–	–	–	–	0.20	0.22	1.12	–
Polyacrylates	–	0.04	1.5	1.0	0.2	1.43	2.40	1.68	80.3

[a] The mass percentages of PMTFPS-MAI for preparation of P1, P2, P3, P4 and P5 were 10%, 20%, 30%, 40% and 50%, respectively.

for 3 h at 0 °C, and then for 24 h at room temperature to obtain PMTFPS-MAI. The copolymerization of PMTFPS-MAI with MMA, BA, and HEMA was carried out under N_2 protection in BAE and MIBK (1:1, w/w) at 65 °C for 12 h. The resulting PMTFPS–*b*-polyacrylate copolymers were precipitated in methanol and vacuum-dried at 40 °C. The detailed compositions and yields of the PMTFPS–*b*-polyacrylate copolymers are shown in Table 1. Based on the mass percentages of PMTFPS-MAI (i.e. 10%, 20%, 30%, 40% and 50%) used during the preparation, the samples are designated as P1, P2, P3, P4 and P5, respectively. For comparison, the polyacrylates were prepared by free-radical polymerization of MMA, BA and HEMA using AIBN (1.5 wt% in all monomers) as an initiator in BAE and MIBK (1:1, w/w) solution at 80 °C for 5 h.

A given amount of the PMTFPS–*b*-polyacrylate copolymer combined with the curing agent (hexamethylene diisocyanate trimer) was dissolved in EA to obtain the copolymer solution at 10 wt% concentration. The copolymer film was prepared by dropping 300 μL of the copolymer solution onto a polished Al plate (20 mm × 20 mm) and allowing the solvent to evaporate completely at ambient temperature in dry air; the plate was then heated in an oven at 110 °C for 2 h. The thickness of the copolymer film was controlled at around 50 ± 5 μm.

2.3. Characterization of the PMTFPS–b-polyacrylate copolymers

Fourier transformed infrared spectroscopy (FT-IR) spectra of samples were recorded in a Spectrum 100 FT-IR spectrometer (PerkinElmer, USA) in the range from 4000 cm^{-1} to 500 cm^{-1} using KBr pellet technique. A small amount of the copolymer solution in EA was dropped on the KBr disk to form a thin film for the measurement. Proton-nuclear magnetic resonance (^1H NMR) analysis was carried out in Varian machines (INOVA 500 MHz and Infinity plus 300WB, USA) by dissolving the samples in deuteriochloroform.

The average relative molar mass and its distribution were determined in gel permeation chromatography (GPC, TDA305, Malvern Instruments Ltd., UK). THF was used as the eluent with a flow rate of 1.0 mL/min at 40 °C. Calibration curve was made by PS standard. Differential scanning calorimetry (DSC) was measured with a Diamond differential scanning calorimeter (Perkin-Elmer, USA) under N_2 atmosphere at a heating rate of 10 °C min^{-1} from −150 °C to 150 °C.

Copolymer morphologies were observed with transmission electron microscope (TEM) (Tecnai G2 F20 200 kV, the Netherlands). Samples for TEM characterizations were prepared by direct dropping of a drop of 1 wt% PMTFPS–*b*-polyacrylate copolymer solution in EA on the carbon-coated copper grids. The solvent was allowed to evaporate at room temperature for 24 h.

Atomic force microscope (AFM) images were obtained using tapping mode on a CSPM5500A of Ben Yuan Ltd., China, equipped with E-type vertical engage piezoelectric scanner. The samples were prepared by spin-coating the copolymer solutions together with the curing agent (10 wt% in EA) onto freshly cleaned silicon wafers and then the films were heated in oven for 2 h at 110 °C. The spinning speed was set at 600 rpm (6 s) and 3000 rpm (10 s) for the first and second steps, respectively.

Surface composition by X-ray photoelectron spectroscopy (XPS) was investigated using a PerkinElmer PHI 5000 C ECSAX-ray photoelectron spectroscopy in ultra-high vacuum with Al K radiation (1486.6 eV) operating at 24.2 W under a vacuum less than 5×10^{-8} Torr at 45°. The tested area was a circle with diameter of 100 μm.

Water contact angles and contact angle hysteresis of the copolymer films were measured by an optical contact angle meter (JC2000D, Shanghai Zhongchen Equipment Ltd., China) at room temperature and ambient humidity. The measurement of contact angle hysteresis was carried out using 5 μL water droplets which expanded and shrunk by 10 μL at 0.1–1.0 μL/s via a needle from a syringe. Images of the droplets were captured by a CCD camera and analyzed to obtain the advancing and receding contact angles, and values of the water contact angle hysteresis were calculated. The surface energy was also calculated according to the equation by Owens–Wendt–Kaelble method [28]. All the contact angles presented are average of at least five or six measurements.

The delayed icing test was performed on a cooling stage under N_2 atmosphere at a constant working temperature of −15 °C. In order to ensure that the surfaces reach a temperature of −15 °C, the sample surfaces were tightly attached to the cooling stage, and a certain time period was required for temperature equilibrium before testing. Water droplets (6 μL) were placed on the sample surfaces by an injector needle tube. The whole freezing process was captured by a high speed CCD camera.

The ice adhesion strength of PMTFPS–*b*-polyacrylate copolymer films was measured on a home built cooling stage which could hold a 4 × 4 array of samples [29]. The cylindrical glass columns were treated with 1*H*,1*H*,2*H*,2*H*-perfluorooctyltrichlorosilane vapor to reduce their surface energies and prevent the water from leaking. As shown in Fig. 2, the coated Al plates (20 mm × 20 mm) were placed onto the cooling stage and let the copolymer film upwards. A small amount of water was filled in between the plate and the stage, and the then frozen water ensures the firm attachment of the sample. The glass columns were put on the Al plates and filled with 450 μL of fresh deionized water. Each column had a contact area with the Al plate of approximately 78.5 mm^2. The cooling stage was covered by an organic glass box which was purged with nitrogen gas to decrease the humidity. The temperature of the stage was reached to −15 °C at a rate of 2 °C/min and was maintained for 3 h. A force transducer (Imada ZP-500 N, Japan) was mounted on a motion stage which moved forward at a rate of 0.5 mm/s to the glass columns. The maximum force was recorded for determining the ice adhesion strength by dividing the area between ice and the contact polymer surface. The average values and the standard deviation were obtained from nine parallel samples.

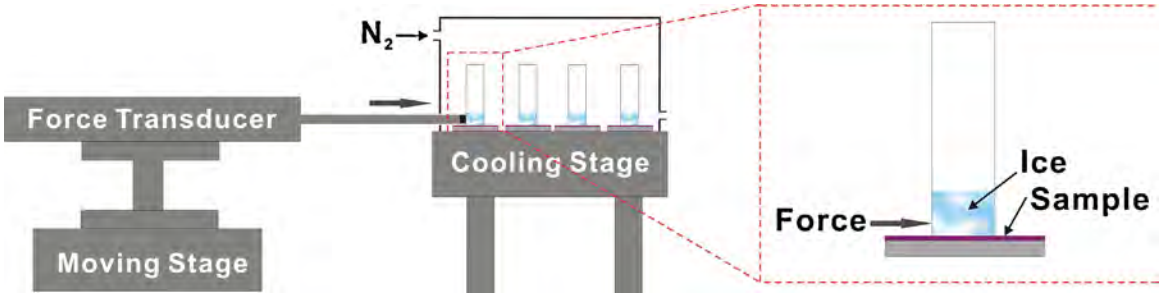

Fig. 2. Schematic depiction of ice shear stress measurement. Al plate (20 mm × 20 mm) which was coated by copolymer was placed onto the cooling stage. The glass column was put on the Al plate and filled with 450 μL of fresh deionized water. The temperature of the stage was reached to −15 °C at a rate of 2 °C/min. The maximum force was recorded for calculating the ice shear stress by a force transducer which was mounted on a motion stage.

3. Results and discussion

To investigate the relationship between the icephobic properties and surface structure of the copolymers, the optimal PMTFPS content for icephobic application was evaluated by synthesizing five block copolymers with different compositions. It was hypothesized that the incorporation of PMTFPS could improve the hydrophobic and icephobic properties of the copolymers. In order to determine the effect of PMTFPS, the microphase-separated structure, surface chemical composition, and icephobic properties of copolymer films were evaluated and discussed in the following sections.

3.1. Synthesis of PMTFPS–b-polyacrylate copolymers

Fig. 3 shows the FT-IR spectra of PMTFPS-MAI and PMTFPS–*b*-polyacrylate (P2). The appearance of peak at 1730 cm^{-1} by the C=O stretching vibration in the spectrum of PMTFPS-MAI (Fig. 3(a)) indicated successful synthesis of PMTFPS-MAI. The characteristic absorption bands of the OH group were observed at 3530 cm^{-1} in the spectrum of PMTFPS–*b*-polyacrylate (Fig. 3(b)), and the strong absorption peak at 1730 cm^{-1} was assigned to the C=O stretching vibration. The peaks at 1265 cm^{-1} and 1213 cm^{-1} were attributed to Si–CH_3 and Si–$CH_2CH_2CF_3$, respectively, which were characteristic signals of PMTFPS. The absorption peak in the range of 1010–1123 cm^{-1} was assigned to Si–O–Si asymmetric stretching vibrations. The peak at 1640 cm^{-1}, which was attributed to the stretching vibration of C=C group, was not detected in the spectrum of PMTFPS–*b*-polyacrylate (Fig. 3(b)), indicating that the monomers were converted in polymerization.

Fig. 4 presents the ^{1}H NMR spectra of PMTFPS-MAI and PMTFPS–*b*-polyacrylate (P2). The peak at 4.06 ppm for PMTFPS-MAI (Fig. 4(a)), attributed to the methylene protons adjacent to the OH group, confirmed successful esterification of PMTFPS-OH and that PMTFPS-MAI was synthesized. The peaks at 2.0 ppm and 0.1 ppm in the spectrum of PMTFPS–*b*-polyacrylate (Fig. 4(b)) were characteristics of methylene next to CF_3 and methyl protons next to Si in PMTFPS, respectively. The peaks of resonance at 3.6–4.0 ppm were attributed to the methylene protons close to the oxygen atom of ester bond. No proton peaks for the double bond of MMA, BA and HEMA were detected in the ^{1}H NMR spectrum of PMTFPS–*b*-polyacrylate.

The GPC traces of the PMTFPS–*b*-polyacrylate copolymers are presented in Fig. 5, and the relative molar mass and polydispersity index (PDI) of the copolymers are summarized in Table 1. The relative number-average molar mass of the copolymers ranged from 1.52×10^4 to 3.23×10^4 and decreased gradually from sample P1 to sample P5 as the amount of PMTFPS-MAI increased. In this study, the content of each monomer was fixed at the same level for all of the five copolymers while the amount of PMTFPS-MAI was varied (Table 1). The gradual increase of PMTFPS-MAI content from sample P1 to sample P5 resulted in a relatively decrease in the amount of the acrylate monomers incorporated into the copolymer chains. Therefore, the relative molar mass of sample P5, which had the largest content of PMTFPS-MAI, was the smallest among the evaluated copolymer samples. The GPC curves of the resulting PMTFPS–*b*-polyacrylate copolymers were monomodal with no shoulder peaks. The copolymers had relatively lower PDI values of 1.59–1.81 (Table 1).

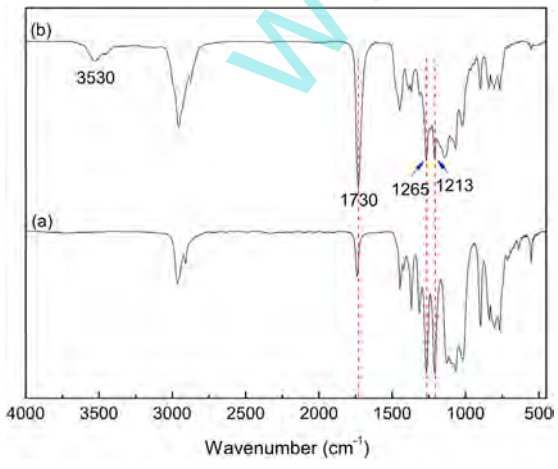

Fig. 3. FT-IR spectra of PMTFPS-MAI (a) and PMTFPS–*b*-polyacrylate (b).

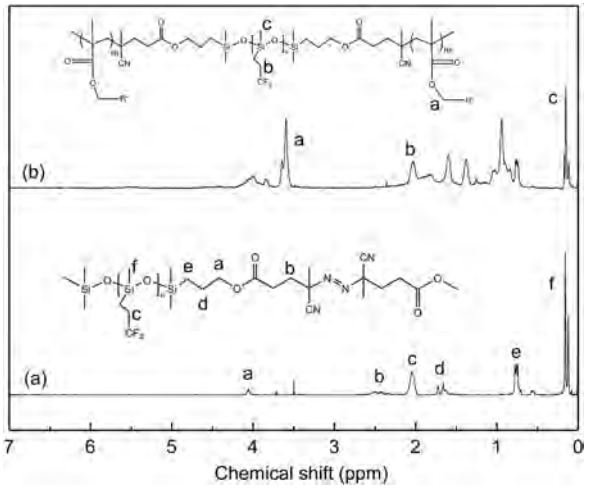

Fig. 4. ^{1}H NMR spectra of PMTFPS-MAI (a) and PMTFPS–*b*-polyacrylate (b).

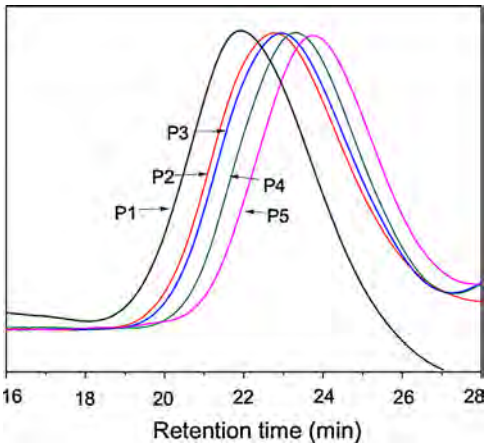

Fig. 5. GPC curves of the PMTFPS–*b*-polyacrylate copolymers.

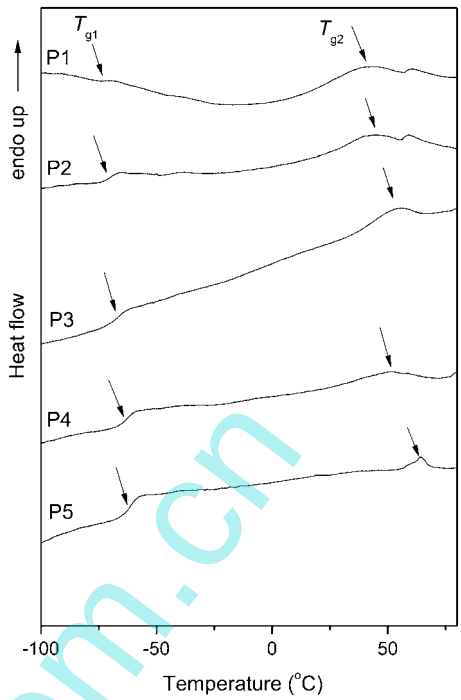

Fig. 6. DSC curves of the PMTFPS–*b*-polyacrylate copolymers.

3.2. Microphase separation

The thermal transitions of the PMTFPS–*b*-polyacrylate copolymers were investigated by DSC (Fig. 6). Two T_g values were observed for all the copolymers. Glass transition temperature at about −70 °C to −61 °C (T_{g1}) attributed to the PMTFPS block was observed in all the copolymer thermograms, indicating that the PMTFPS block is flexible at low temperature [24]. Polyacrylate

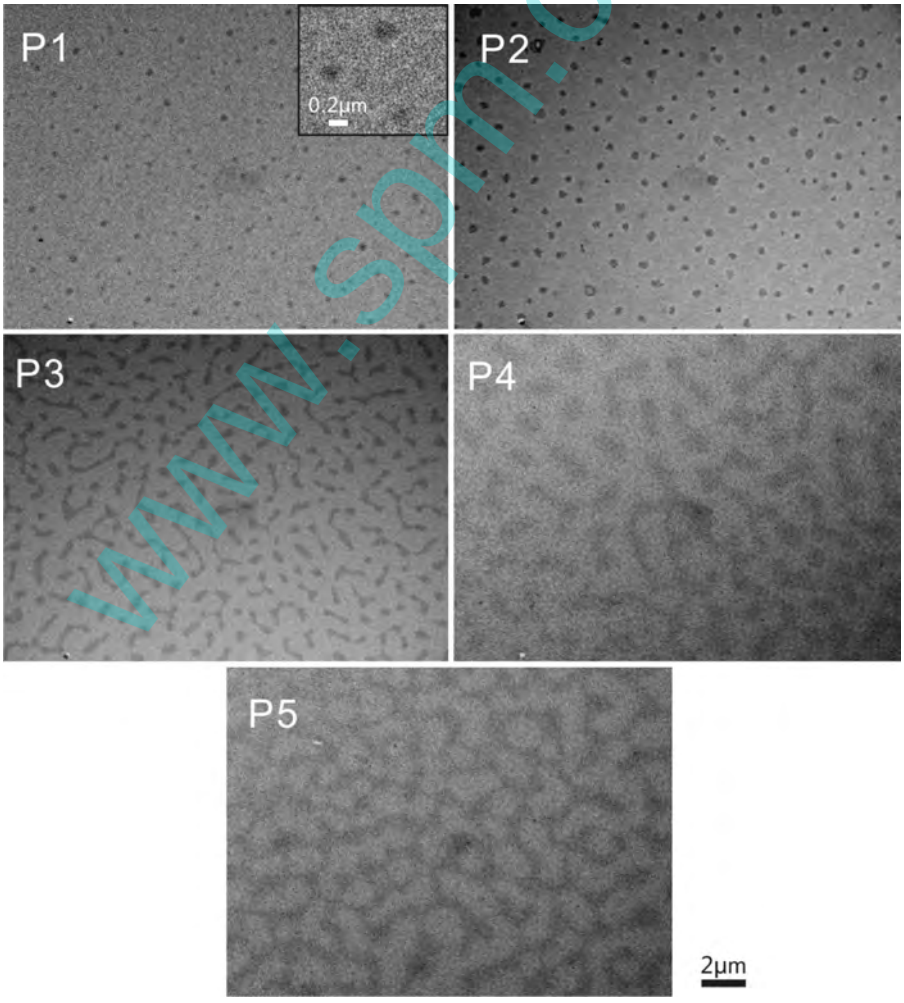

Fig. 7. TEM micrographs of PMTFPS–*b*-polyacrylate copolymers.

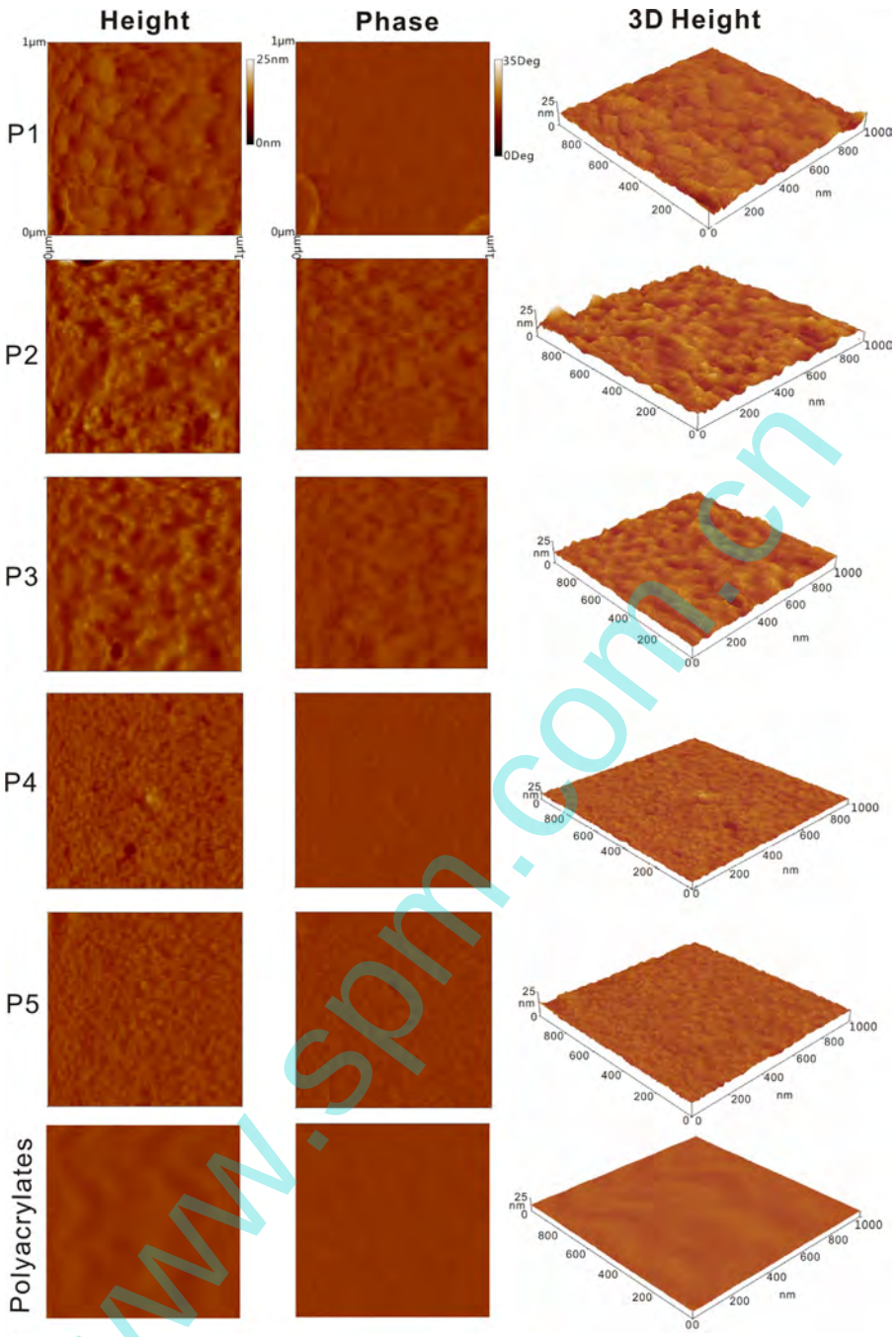

Fig. 8. AFM images of PMTFPS–*b*-polyacrylate films.

block displayed its T_{g2} at about 46–64 °C, which was higher than that of PMTFPS. The DSC results suggested there were possibly incompatible components in the copolymers that could lead to microphase separation.

The bulk morphologies of the PMTFPS–*b*-polyacrylate copolymers were investigated via TEM. The high electron density of the PMTFPS block, as compared with polyacrylate, provided sufficient contrast for TEM observation without the need of special staining techniques. Microphase separation would occur because of the thermodynamic incompatibility between the PMTFPS and polyacrylate domains. Furthermore, the incorporation of the fluorinated alkyl group into the polysiloxane chain could enhance microphase separation between the PMTFPS and the polyacrylate blocks [30]. As shown in Fig. 7, all the PMTFPS–*b*-polyacrylate copolymers had microphase separated structures with clear interfaces. For the copolymers with the lowest PMTFPS content (P1), the spherical PMTFPS phase dispersed in the continuous polyacrylate matrix. When the PMTFPS content increased to 20 wt% (P2), the dispersed spherical PMTFPS phase was bigger than that of the sample P1. Further increasing the PMTFPS content to 30 wt% (P3), the PMTFPS phase exhibited ribbonlike structure. When the PMTFPS content was further increased to 40 wt% (P4) or 50 wt% (P5), a double continuous phase structure emerged. From the TEM micrographs, the microphase separation of the copolymers would be associated with the composition and relative molar mass of the PMTFPS–*b*-polyacrylate copolymers. The relative molar mass of the PMTFPS–*b*-polyacrylate copolymers decreased with the increased content of PMTFPS; the macromolecules would be dispersed easier with a lower relative molar mass. Therefore, from sample P1 to P5, the PMTFPS related regions became larger and changed from

Table 2
Element compositions of the copolymer surfaces obtained by XPS and their surface roughness (R_q) analyzed by AFM.

Sample	C (atomic %)	O (atomic %)	F (atomic %)	Si (atomic %)	F/Si	O/Si	R_q (nm)
P1	49.9	18.1	18.7	13.2	1.42	1.37	0.97
P2	46.7	14.7	25.9	12.6	2.05	1.16	1.56
P3	45.9	14.4	28.8	10.9	2.64	1.29	1.18
P4	50.1	18.9	17.6	13.5	1.30	1.40	0.86
P5	48.7	17.8	19.5	14.0	1.39	1.27	0.71
PMTFPS[a]	–	–	–	–	3.00	1.00	–
Polyacrylates	74.8	25.2	–	–	–	–	0.34

[a] The F/Si and O/Si data of PMTFPS are obtained from its chemical structure theoretically.

spherical to double continuous phase with the increased PMTFPS content.

Given that the surface morphology would have a significant influence on the icephobic behaviors of the copolymer films [20], the surface morphologies of PMTFPS–*b*-polyacrylate copolymer films were investigated by AFM. Because of the low surface energy of fluorosilicones, the PMTFPS block tended to migrate to the surface of the copolymer; thus, the surface morphologies of the copolymer films would be different from those of the bulk. As shown in Fig. 8, the surface morphology of P1 was characterized by an irregular fold structure. However, the surfaces of P2 and P3 displayed discontinuous nanostructures. On the other hand, wormlike surface nanostructures were observed for the surfaces of P4 and P5. The PMTFPS phase with a lower surface energy appeared on the top layer of the copolymer films, whereas the polyacrylate phase appeared at the bottom of the films. In the AFM phase images, microphase separation was more clearly observed for P2 and P3 than for P1, P4 and P5. Compared to the PMTFPS–*b*-polyacrylate copolymer films, the surface of the plain polyacrylate film was flat and the microphase separation morphology was not obvious. Because of the thermodynamic incompatibility of the segments of the block copolymers, the PMTFPS blocks tended to be assembled into larger area and formed a rough surface. From Table 2, it could be seen that the surface roughness of the sample P2 was 1.56 nm, which was bigger than that of the other samples.

3.3. Surface composition

In addition to the surface morphology, the surface elemental composition also has a marked impact on the surface wettability and icephobic properties of copolymer coatings [31,32]. The surface elemental compositions of the PMTFPS–*b*-polyacrylate copolymer films were evaluated from the XPS spectra (Fig. 9). The carbon, oxygen, fluorine and silicon content as well as the atomic relative ratios are summarized in Table 2. The peaks in Fig. 9 at 284.4 eV, 534.8 eV, 690.9 eV and 104.8 eV arose from C1s, O1s, F1s and Si2p core levels, respectively. It proved that the surface of the sample P2 was mainly covered by PMTFPS, and the effect of polyacrylate component on sample P2 surface was lower than that of the other film surfaces. It could be seen from Table 2 that the amount of oxygen on the surface of polyacrylates was much higher than that on the PMTFPS–*b*-polyacrylate copolymer film surface, which indicated a higher interaction of polyacrylates with water molecules due to the hydrogen bond between them. Based on the presented XPS and AFM results, it is suggested that the surface roughness could be enhanced by the enrichment of PMTFPS blocks on the copolymer surface. The AFM images confirm the biggest surface roughness of sample P2 in all the samples. Table 2 also shows the F/Si values were greater than 1 but less than the theoretical value of 3 of PMTFPS, and the F/Si values of sample P2 and P3 were higher than those of samples P1, P4 and P5. The interaction between the fluorine and silicon atoms limited the migration of the fluoride group to the sample surface.

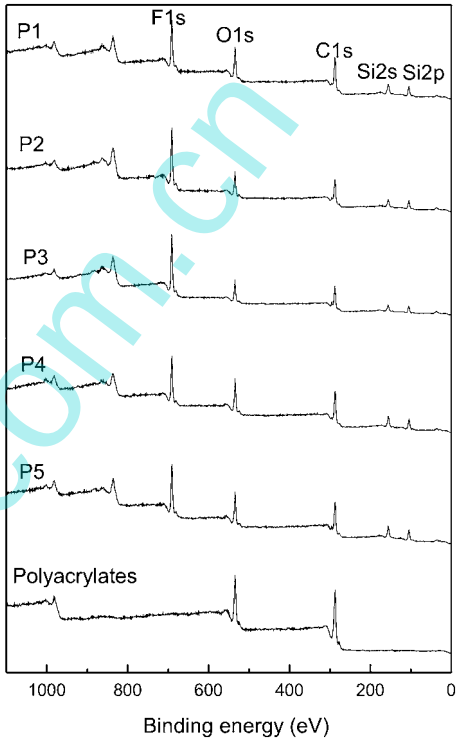

Fig. 9. XPS survey spectra of PMTFPS–*b*-polyacrylate films.

3.4. Contact angles and surface energy

The water contact angles, contact angle hysteresis and surface energies of the PMTFPS–*b*-polyacrylate copolymer films are listed in Table 3. The water contact angles of the five copolymer films were approximately 100.3 ± 0.7°, which were higher than that of the polyacrylates (91.2 ± 0.7°) and presented good hydrophobicity. The trifluoropropyl groups in PMTFPS migrated to the surface of the copolymer; as confirmed by XPS detection; this would improve the water repellency of the copolymer films. According to the reference [24], the surface energy of PMTFPS was 21.4 mJ m^{-2}. The enrichment of PMTFPS on copolymer surface would reduce the surface energy of the films. The surface energies of the copolymer films

Table 3
Water contact angles, contact angle hysteresis and surface energies.

Sample	Static contact angle (°)	Contact angle hysteresis (°)	Surface energy (mJ m^{-2})
P1	99.1 ± 0.8	30.5 ± 2.4	23.83
P2	100.9 ± 1.2	21.8 ± 1.7	21.49
P3	100.7 ± 1.5	26.5 ± 1.1	22.50
P4	100.5 ± 1.3	28.7 ± 2.9	22.91
P5	100.7 ± 1.7	36.1 ± 0.9	23.35
Polyacrylates	91.2 ± 0.7	48.8 ± 1.7	28.57

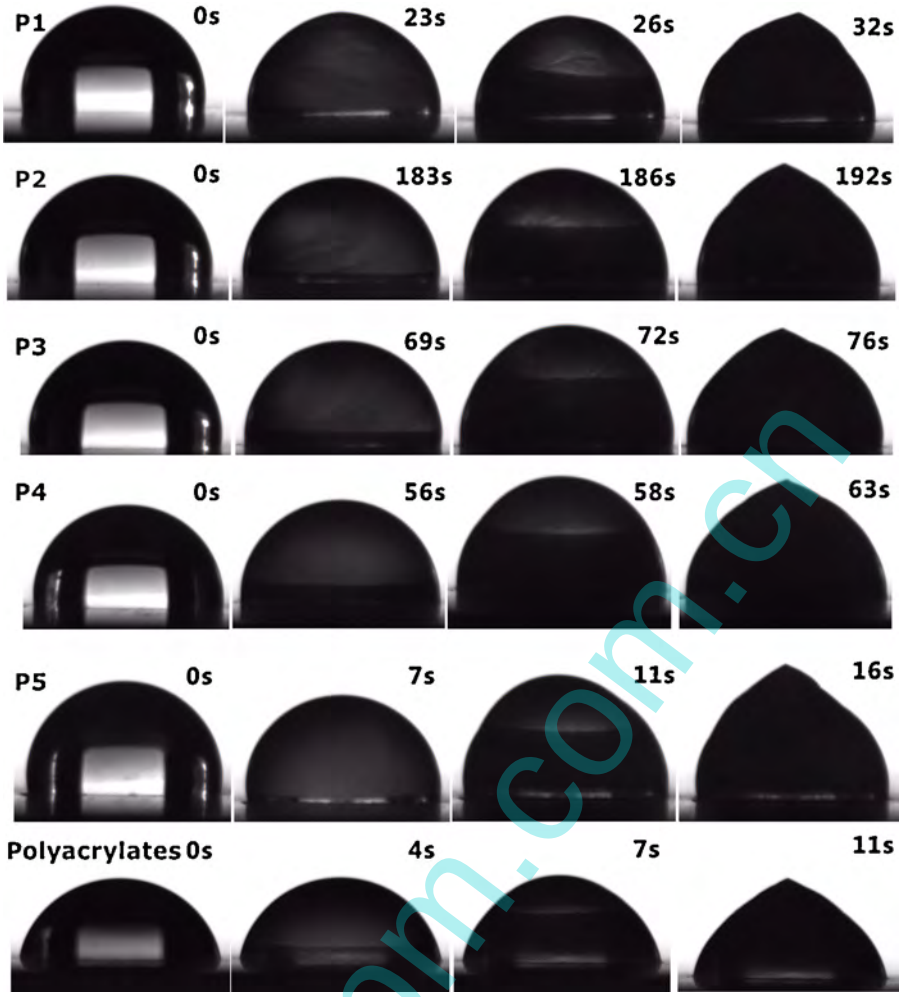

Fig. 10. Freezing time of water droplet on the surface of block copolymer films at −15 °C.

(Table 3) were approximately 22.8 ± 0.9 mJ m^{-2}, which were lower than that of polyacrylates (28.5 mJ m^{-2}) and were close to the surface energy of PMTFPS.

Although the contact angles and surface energies of the copolymer films were almost the same, the values of contact angle hysteresis were distinctly different. Generally, contact angle hysteresis is quantified as the discrepancy between the advancing and receding contact angles. This parameter is important for assessing the icephobic properties and is dependent on both the topographical structure and the chemical compositions of the copolymer [9]. The contact angle hysteresis varied within 21–36° for all the samples; these values were lower than that of polyacrylates (48.8 ± 1.7°); the contact angle hysteresis of sample P2 was the lowest among all the samples. The low contact angle hysteresis of P2 could be attributed to the enrichment of PMTFPS on the copolymer surface, which would reduce the strength of hydrogen bond between the polymer surface and water. The synergistic effect of silicone and fluorine groups that could decrease the interaction with water could contribute to decreasing the contact angle hysteresis.

3.5. Icephobic properties

3.5.1. Delayed icing time

To investigate the icephobic property of the PMTFPS–*b*-polyacrylate copolymer films, the delayed icing test was conducted. Fig. 10 shows water freezing process on the different copolymer film surfaces at −15 °C. Initiation freezing of the water droplet is indicated by the transparent center of water droplets becoming opacity. The delayed icing time is defined as the time that the drop changed from transparent to opaque. Freezing of the water droplet on the copolymer film surface was initiated at 23 s, 183 s, 69 s, 56 s and 7 s, respectively, for the P1–P5 films, all of which were longer than that on the polyacrylates film surface (4 s). These results indicate that the PMTFPS–*b*-polyacrylate copolymers were remarkably effective in delaying icing. The longest delay time was achieved with sample P2, attributed to the large discontinuous nanostructures and bigger surface roughness. Bigger surface roughness could increase the distance between water and the copolymer; thus, heat transfer via the water-surface interface could be delayed.

3.5.2. Ice shear strength

The ice shear strength was also measured to explore the icephobic property of the PMTFPS–*b*-polyacrylate copolymers. Fig. 11 shows the ice shear strengths on the PMTFPS–*b*-polyacrylate copolymer surfaces. The ice shear strengths on the copolymer films varied in range of 301–551 kPa and the lowest value (301 ± 10 kPa) was observed for sample P2. For comparisons, the ice shear strengths of the polyacrylates film and a commercial polyacrylate-polyurethane (PU) coating were also measured, with values of 804 ± 37 kPa and 1005 ± 69 kPa, respectively, which were significantly higher than that of the PMTFPS–*b*-polyacrylate copolymer films. The high ice shear strength on polyacrylates surface is mainly

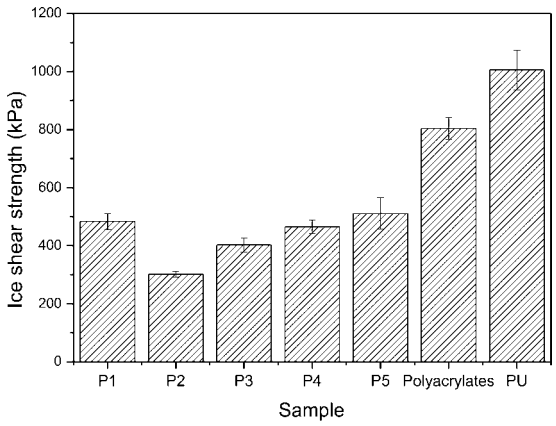

Fig. 11. Ice shear strength of PMTFPS–*b*-polyacrylate films.

associated with the hydrogen bond between the surface and the ice. PMTFPS chains with low surface energy can readily migrate to the air interface of the copolymer film, and the low T_g of PMTFPS results in flexibility at low temperature that is beneficial for decreasing the ice shear strength. The lowest ice shear strength of sample P2 is primarily attributed to the low content of polyacrylate blocks on the copolymer surface, which would result in strong hydrogen bond. In addition, the synergistic effect of fluorine and silicon groups on the copolymer surface could also reduce the ice shear strength. The high F/Si values of the samples P2 and P3 (2.05 and 2.64) can result in an enhanced synergistic effect of fluorine and silicon compared with the other samples, thereby affecting the ice shear strength.

An interesting correlation between the ice shear strength of the PMTFPS–*b*-polyacrylate copolymers and the water contact angle hysteresis was observed, whereby a lower water contact angle hysteresis was associated with lower ice shear strength; sample P2 with the lowest contact angle hysteresis (21.8°) had the lowest shear strength.

Based on the AFM data (Fig. 8), it was concluded that the PMTFPS–*b*-polyacrylate copolymers showed microphase separation structures; the surface roughness of sample P2 was 1.56 nm, which was bigger than those of the other samples (Table 2). The bigger surface roughness could lead to a small contact area between water and polyacrylate when water contact with the film surface of sample P2, resulting in weaker hydrogen bond between them. According to the literature [8], the icephobic property of the superhydrophobic surface is depressed in humid atmosphere when water is condensed on a rough surface. In addition, the mechanical interlocking on superhydrophobic surface with a high surface roughness (usually micron scale) further increases the ice adhesion strength [10]. Compared with the superhydrophobic surface, the nanostructure morphology of PMTFPS–*b*-polyacrylate copolymer presented a relatively smoother surface, and the effect of mechanical interlocking between ice and the copolymer surface on the ice shear strength was trivial and thus could be neglected. From the ice shear strength test, it is deduced that copolymers based on the PMTFPS modified polyacrylate present reduced ice adhesion strength and exhibited good icephobic property.

4. Conclusions

The fluorosilicone-containing block copolymers (PMTFPS–*b*-polyacrylate) were synthesized using PMTFPS-MAI in 10–50 wt%. When the content of PMTFPS-MAI was 20 wt% (sample P2), the delayed icing time was 186 s at −15 °C, and the ice shear strength was 301 ± 10 kPa, which was significantly lower than that of the polyacrylates (804 ± 37 kPa). AFM and XPS demonstrated that the delayed icing time was related to the surface roughness and enrichment of PMTFPS blocks on the copolymer surface; synergistic effect of silicone and fluorine could reduce the ice shear strength. Thus, the PMTFPS–*b*-polyacrylate copolymer can be a good candidate for icephobic applications.

Acknowledgment

This work is financially supported by National Natural Science Foundation of China via nos. 51273146 and 51103061.

References

[1] C.C. Ryerson, Ice protection of offshore platforms, Cold. Reg. Sci. Technol. 65 (2011) 97–110.
[2] Y. Wang, J. Xue, Q. Wang, Q. Chen, J. Ding, Verification of icephobic/anti-icing properties of a superhydrophobic surface, ACS Appl. Mater. Interfaces 5 (2013) 3370–3381.
[3] M.A. Sarshar, C. Swarctz, S. Hunter, J. Simpson, C. Cho, Effects of contact angle hysteresis on ice adhesion and growth on superhydrophobic surfaces under dynamic flow conditions, Colloid. Polym. Sci. 219 (2013) 427–435.
[4] M. Ruan, W. Li, B. Wang, B. Deng, F. Ma, Z. Yu, Preparation and anti-icing behavior of superhydrophobic surfaces on aluminum alloy substrates, Langmuir 29 (2013) 8482–8491.
[5] K.R. Khedir, G.K. Kannarpady, H. Ishihara, J. Woo, M.P. Asar, C. Ryerson, A.S. Biris, Temperature-dependent bouncing of super-cooled water on Teflon-coated superhydrophobic tungsten nanorods, Appl. Surf. Sci. 279 (2013) 76–84.
[6] H. Li, Y.H. Zhao, X.Y. Yuan, Facile preparation of superhydrophobic coating by spraying a fluorinated acrylicrandom copolymer micelle solution, Soft Matter 9 (2013) 1005–1009.
[7] K.K. Varanasi, T. Deng, J.D. Smith, M. Hsu, N. Bhate, Frost formation and ice adhesion on superhydrophobic surfaces, Appl. Phys. Lett. 97 (2010) 234102.
[8] S. Farhadi, M. Farzaneh, S.A. Kulinich, Anti-icing performance of superhydrophobic surfaces, Appl. Surf. Sci. 257 (2011) 6264–6269.
[9] H. Stone, Ice-phobic surfaces that are wet, ACS Nano 6 (2012) 6536–6540.
[10] J. Chen, J. Liu, M. He, K. Li, D. Cu, Superhydrophobic surfaces cannot reduce ice adhesion, Appl. Phys. Lett. 101 (2012) 111603.
[11] S. Yang, Q. Xia, L. Zhu, J. Xue, Q. Wang, Q. Chen, Research on the icephobic properties of fluoropolymer-based materials, Appl. Surf. Sci. 257 (2011) 4956–4962.
[12] M. Susoff, K. Siegmann, C. Pfaffenroth, M. Hirayama, Evaluation of icephobic coatings-screening of different coatings and influence of roughness, Appl. Surf. Sci. 182 (2013) 870–879.
[13] H. Wang, G. He, Q. Tian, Effects of nano-fluorocarbon coating on icing, Appl. Surf. Sci. 258 (2012) 7219–7224.
[14] Y. Huang, M. Hu, S. Yi, Preparation and characterization of silica/fluorinated acrylate copolymers hybrid films and the investigation of their icephobicity, Thin Solid Films 520 (2012) 5644–5651.
[15] L. Zhu, J. Xue, Y. Wang, Q. Chen, J. Ding, Q. Wang, Ice-phobic coatings based on silicon-oil-infused polydimethylsiloxane, ACS Appl. Mater. Inter. 5 (2013) 4053–4062.
[16] J. Li, Y. Zhao, J. Hu, Anti-icing performance of a superhydrophobic PDMS/modified nano-silica hybrid coating for Insulators, J. Adhes. Sci. Technol. 26 (2012) 665–679.
[17] F. Arianpour, M. Farzaneh, S.A. Kulinich, Hydrophobic and ice-retarding properties of doped silicone rubber coatings, Appl. Surf. Sci. 265 (2013) 546–552.
[18] E. Pouget, J. Tonnar, P. Lucas, P. Desmazes, F. Ganachaud, B. Boutevin, Well-architectured poly(dimethylsiloxane)-containing copolymers obtained by radical chemistry, Chem. Rev. 110 (2010) 1233–1277.
[19] G. Momen, M. Farzaneh, R. Jafari, Wettability behaviour of RTV silicone rubber coated on nanostructured aluminium surface, Appl. Surf. Sci. 257 (2011) 6489–6493.
[20] D.M. Yu, Y.H. Zhao, H. Li, H.Z. Qi, B. Li, X.Y. Yuan, Preparation and evaluation of hydrophobic surfaces of polyacrylate-polydimethylsiloxane copolymers for anti-icing, Prog. Org. Coat. 76 (2013) 1435–1444.
[21] R. Menini, M. Farzaneh, Advanced icephobic coatings, J. Adhes. Sci. Technol. 25 (2011) 971–992.
[22] H. Murase, K. Nanishi, H. Kogure, T. Fujibayashi, K. Tamura, N. Haruta, Interactions between heterogeneous surfaces of polymers and water, J. Appl. Polym. Sci. 54 (1994) 2051–2062.
[23] S.V. Perz, C.S. McMillan, M.J. Owen, Wettability of fluorosilicone surfaces, in: D.G. Castner, D.W. Grainger (Eds.), Fluorinated Surfaces, Coatings, and Films, Washington, DC, 2001, pp. 112–128.
[24] M.J. Owen, A review of significant directions in fluorosiloxane coatings, Surf. Coat. Int. 87 (2004) 71–148.
[25] C. Liu, C.P. Hu, Synthesis, characterization and *in vitro* oxidative stability of poly(3,3,3-trifluoropropyl)methylsiloxane modified polyurethaneurea, Polym. Degrad. Stabil. 94 (2009) 259–266.

[26] S. Haseloh, P.V.D. Schoot, R. Zentel, Control of mesogen configuration in colloids of liquid crystalline polymers, Soft Matter 6 (2010) 4112–4119.
[27] B. Li, D. Majonis, P. Liu, M.A. Winnik, Synthesis and characterization of a naphthalimide-dye end-labeled copolymer by reversible addition-fragmentation chain transfer (RAFT) polymerization, Can. J. Chem. 89 (2011) 317–325.
[28] H. Fang, S. Zhou, L. Wu, Microphase separation behavior on the surfaces of PEG-MDI-PDMS multiblock copolymer coatings, Appl. Surf. Sci. 253 (2006) 2978–2983.
[29] A.J. Meuler, J.D. Smith, K.K. Varanasi, J.M. Mabry, G.H. Mckinley, R.E. Cohen, Relationships between water wettability and ice adhesion, ACS Appl. Mater. Interfaces 2 (2010) 3100–3110.
[30] L.M. Yi, C.X. Huang, W. Zhou, Synthesis, surface properties, and morphologies of poly[methyl(3,3,3-trifluoropropyl)siloxane]-*b*-polystyrene-*b*-poly(*tert*-butyl acrylate) triblock copolymers by a combination of anionic ROP and ATRP, J. Polym. Sci. Polym. Chem. 50 (2012) 1728–1739.
[31] K. Lian, C. Chen, H. Liu, N. Wang, H. Yu, Z. Luo, Surface microphase separation in PDMS-*b*-PMMA-*b*-PHFBMA triblock copolymer films, J. Appl. Polym. Sci. 120 (2011) 156–164.
[32] S.A. Kulinich, M. Farzaneh, On wetting behavior of fluorocarbon coatings with various chemical androughness characteristics, Vacuum 79 (2005) 255–264.